JOURNAL OF MATERIALS SCIENCE **35** (2000) 2255–2262

Physical properties of some iron based alloys in liquid and amorphous states

V. E. SIDOROV
Department of Physics, Ural State Pedagogical University, Ekaterinburg, 620219-CIS, Russia

M. CALVO-DAHLBORG* ‡, U. DAHLBORG‡
Department of Neutron Physics, Royal Institute of Technology, 100 44 Stockholm, Sweden
E-mail: dahlborg@mines.u-nancy.fr

P. S. POPEL, S. CHERNOBORODOVA
Department of Physics, Ural State Pedagogical University, Ekaterinburg, 620219-CIS, Russia

The atomic structure and the physical properties of amorphous ribbons depend strongly on the state of the melt before quench. It is known that slightly above liquidus metallic melts can preserve a non-equilibrium metastable state for a long time. Moreover some structural transformations in liquid metallic alloys, similar to phase transitions in solids, may take place with an increase of the temperature. In this paper we report measurements of the viscosity, magnetic susceptibility and surface tension in some Fe-based melts. Amorphous ribbons of the same alloys were prepared by standard planar method from different states of the melt. The electrical resistivity, the kinetics of crystallization and the magnetic properties of the ribbons were investigated. It was found that the properties depending upon nanoscale inhomogeneities are different for ribbons produced after different heat treatments of the melt before quench.

1. Introduction

A significant improvement has been achieved during the last years in the quality of amorphous metallic materials (metallic glasses) produced by melt spinning. Among the different existing production techniques, melt quenching is, from an industrial point of view, most convenient as it can provide large amounts of amorphous materials in the form of thin but wide ribbons. Furthermore, metallic glasses are of technological interest because of the specific properties they possess as compared to their crystalline counterparts. However, in modern technological production processes, little attention has been paid to the preparation of the melt before quench, as it was early believed that a change in the structure of the melt caused by external forces (low temperature heating, treatment in magnetic fields and by ultrasonic methods, admission of the current through the melt, etc.) only affects the physical properties of the produced amorphous ribbons to a small extent.

The influence of heat treatment of a molten metallic alloy before quench on the structure and the properties of amorphous ribbons has recently been investigated in several works [1, 2]. The effects observed in measurements on several physical properties, like viscosity, resistivity, etc, were explained either by free volume freezing or by deactivation of crystallization centers when the melt was heated far above the liquidus temperature. However, the behavior of some other physical properties of the melts can not be explained by the occurrence of any of these two processes, which indicates that other physical phenomena are involved. As an example, anomalous variations can be observed in "property vs. temperature" curves for some metallic alloys. These anomalies take place in a narrow temperature interval in the liquid phase [3, 4] and they are similar to what is seen in the solid state near phase transitions.

The possibility of structural changes occurring in metallic melts was also indicated in some theoretical model calculations [5–9]. It was shown in [3] that after the melting of the heterogeneous initial alloy, a microheterogeneous melt is formed. One can consider it as a metastable non-equilibrium microemulsion or as a microsuspension of disperse particles enriched in one of the components and surrounded by a molten matrix of different composition. These particles are thus inherited from the initial material. They seem to have sharp but irregular interfaces [4,10] and a more or less homogeneous internal structure and local properties. One can therefore identify them as a disperse phase of the colloidal melt. Small angle neutron scattering experiments have recently revealed the existence of domains in an eutectic melt [10]. The physical reason for the existence of these microheterogeneous regions is the

* Author to whom all correspondence should be addressed.
‡ *Present Address*: Laboratoire de Science et Génie des Matériaux Métalliques, CNRS UMR 7584, Ecole des Mines, 54042 Nancy Cedex, France. E-mail: dahlborg@mines.u-nancy.fr

excess free energy at the interfaces. Thermodynamic calculations have shown that it is energetically favorable for the melt to exhibit spontaneous emulsification of large inclusions of the disperse phase up to a size of the order of 10 to 100 nm. Furthermore, these particles dissolve in the surrounding melt very slowly. It can thus be expected that there exists a wide range of particle sizes if the interface tension, σ, at their boundaries increases with decreasing radius R faster than R^{-2}. According to [3], such a behavior of σ is necessary in order to maintain the energy balance between a particle and the surrounding melt.

When heating the melt to a temperature, which is characteristic for its composition, the thermodynamic equilibrium between the particles and the melt matrix is destroyed and the system irreversibly transforms to a true solution state which is thermodynamically stable at all the above-liquidus temperatures. This transformation may be sharp but can also take place via several steps in the dispersion of the particles to smaller ones even in simple binary systems [4]. If the melt consists of three components or more, a set of disperse particles with various composition can exist in the microheterogeneous melt and each kind of particles start to dissolve at specific temperatures.

In addition to the microheterogeneity on the colloidal scale (we shall call it a "meso-scale" microheterogeneity), there are small domains in the system where the short-range order differs from the surroundings. The size of these domains does not exceed 1 to 2 nm, their internal structure is varying in the radial direction and their boundary is probably smooth [10]. Thus these objects can be identified as "clusters". The main reason for their existence is the non-equal interaction between different kinds of atoms. When heating the melt the internal structure of the clusters changes continuously or via several steps of distinct transformations [11, 12]. In microheterogeneous liquid alloys the transformations of the clusters can take place both inside disperse particles and/or in the surrounding melt.

It can thus be concluded that several different kinds of structural modifications can occur in a melt when the temperature is varied and it is in principle possible to construct a phase diagram also for the liquid state [3, 6, 13]. During rapid quenching some features of the structure of the melt can be inherited by the amorphous ribbon and influence its properties. It may thus be conjectured that metallic amorphous ribbons produced by quench from melts with different structure, i.e. from melts which have undergone different heat treatments, will have different structure and physical properties. As a matter of fact, indications that such a dependence exists are strong [1, 2, 14–17] and an explanation can thus be given to many incompatible results published in the literature so far.

In order to obtain a better understanding of the physical processes responsible for the phenomena briefly outlined above, experimental investigations on the presence and the characteristics of structural transformations in molten $Fe_{85}B_{15}$ and $Fe_{64}Co_{21}B_{15}$ alloys are described in the present paper. Their influence on several physical properties of the melt-spun ribbons with the same composition, but produced from different thermodynamic states of the melt before quench, is also demonstrated. Several different experimental techniques were used for these studies.

2. Experimental investigations of the liquid state

2.1. Sample preparation

The samples were produced from raw materials of technical purity: Fe, ARMCO iron (purity 99.7%), electrolytic Co (purity 99.8%) and B (purity 99.6%). The $Fe_{85}B_{15}$ alloy was prepared by arc-melting of Fe and B while the FeCoB alloy was obtained by vacuum fusion in an alumina crucible in a MF-vacuum induction furnace. In order to remove possible moisture and gases adsorbed in boron and to avoid the composition changes introduced by the degassing of boron, a vacuum furnace IS-01/111 (Leybold, Heraeus) was used. The chemical composition of the produced alloy was checked with the help of the inductive-coupled-plasma spectrometer Jobin-Yvon JY 70 VHR.

Three different physical properties of the molten alloys were measured. The kinematic viscosity, ν, was determined by the oscillating torsion method, the surface tension, σ, by the sessile drop method and the magnetic susceptibility, χ, by the Faraday method. All experiments were carried out in helium atmosphere containing an impurity concentration less than 0.005%. Before every measurement the installations were outgassed down to 10^{-2} Pa and filled with helium. Crucibles of BeO and Al_2O_3 were used. It is necessary to point out that the uncertainty in the shape of the measured curves, as well as the positions and the amplitudes of the irregular features presented below, are mainly determined by accidental errors. The error in every measurement is thus less than 1.5%, 2.0% and 1.0% in the determination of ν, σ and χ, respectively. All experiments were carried out during heating and subsequent cooling with a temperature step of 15 to 20 degrees. In order to obtain a homogeneous temperature field in the samples and thus to measure reliable values of the different physical quantities, all samples were left to equilibrate during 10 to 15 min at each temperature before the measurements were actually performed.

2.2. Results

The measured "property vs. temperature" curves for $Fe_{85}B_{15}$ and $Fe_{64}Co_{21}B_{15}$, shown in Figs 1 to 3, exhibit, for the same property, similar variations. The meaning of the arrows is discussed in Section 3. The most notable characteristics of the data is that the temperature variations of the measured kinematic viscosity, $\nu(T)$, and the surface tension, $\sigma(T)$, are different on heating and on cooling while the magnetic susceptibility, $\chi(T)$, is the same. It is to be noted that all observations are reproducible, i.e. if the alloy is fully solidified down to room temperature and remelted up to the same temperature range, the measured values agree within the experimental errors. The observed effects can thus not be attributed to a possible inhomogeneity of the initial

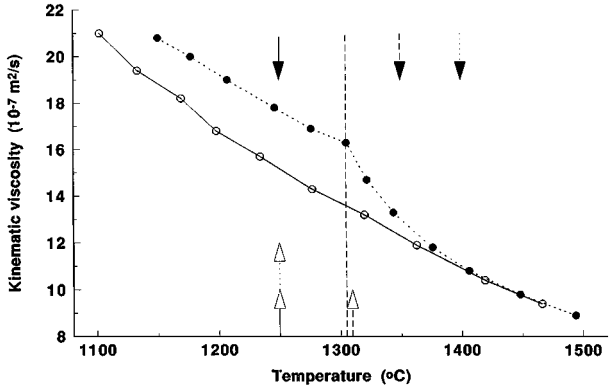

(a)

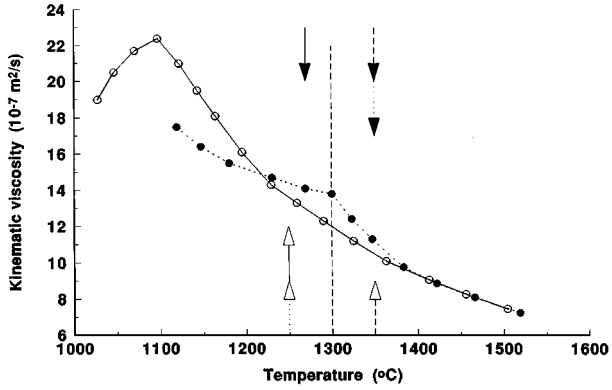

(b)

Figure 1 The temperature dependence of the kinematic viscosity ν for liquid a) $Fe_{85}B_{15}$ and b) $Fe_{64}Co_{21}B_{15}$. ● heating, ○ cooling. The arrows with full head indicate maximum heating temperature of the melt and the arrows with open head the quenching temperatures for samples of series I (full line), of series II (dashed line) and of series III (dotted line). The vertical dashed line indicates the dissolution temperature T_d.

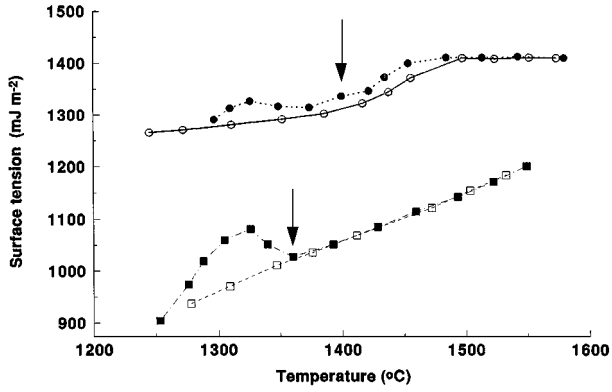

Figure 2 The temperature dependence of the surface tension σ for liquid $Fe_{85}B_{15}$ (■—heating; □—cooling) and $Fe_{64}Co_{21}B_{15}$ (● heating, ○ cooling). The meaning of the arrows is discussed in the text.

solid alloy just after production as this would dissolve on the first heating above its melting point. The values recorded during heating present an anomalous behavior. For example, as is shown in Fig. 1, the viscosity exhibits during heating of both alloys an irregularity near 1300°C while the temperature variation on cooling is smooth. This temperature will in the following be called T_d, the dissolution temperature. The viscosity curves obtained during heating are similar for the two alloys, the measured values for $Fe_{85}B_{15}$ being about 15% larger than the ones for $Fe_{64}Co_{21}B_{15}$. The activation energy is found to be a factor two larger above T_d than below. The curves obtained during cooling are also similar at high temperatures while at low temperatures, i.e. below T_d, the variations are different. The surface tension exhibits a somewhat different temperature behavior for the two alloys as is shown in Fig. 2. However, both curves show an irregular behavior with a pronounced maximum at about T_d on heating while the curves are smooth on cooling. The origin of the other irregularities as well as the flat portion at temperatures above 1500°C is presently not understood. From the temperature variation of the viscosity and of the surface tension another characteristic temperature, T_b, can be defined. The index b stands here for branching and T_b is thus the temperature at which the curves on heating and on cooling are joining. For both alloys, shown in Figs 1 and 2, T_b is about 1500°C.

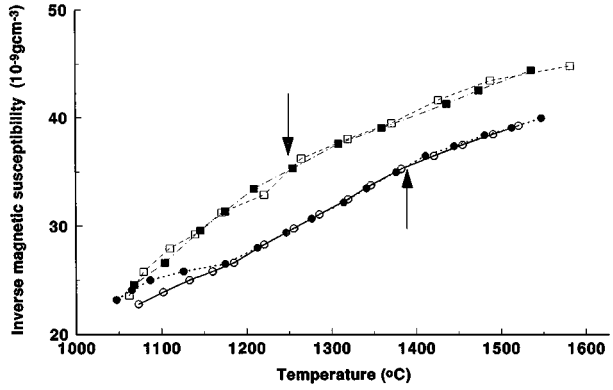

Figure 3 The temperature dependence of the inverse magnetic susceptibility $1/\chi$ for liquid $Fe_{85}B_{15}$ (■—heating; □—cooling) and $Fe_{64}Co_{21}B_{15}$ (● heating, ○ cooling). The meaning of the arrows is discussed in the text.

The temperature dependence of the inverse magnetic susceptibility (Fig. 3) is also very similar for the two alloys. It should be noted that no anomaly in the vicinity of T_d is seen. The kink near 1160°C, is corresponding to the kink at the same temperature in the viscosity curve and it is attributed to the liquidus point. No other difference between the heating and cooling curves is observed. It should though be noted that above the liquidus, the curves might be divided in two linear regions with an intersection just below 1400°C for $Fe_{64}Co_{21}B_{15}$ and near 1250°C for $Fe_{85}B_{15}$.

The results presented above indicate that structural transformations occur in both alloys at T_d, close to 1300°C. From the nature of the three measured quantities shown in Figs 1 to 3, it can be concluded that the length scale involved in these transformations is a hydrodynamic one, i.e. it ranges over several interatomic distances. The results may thus be discussed in the framework of the metastable microheterogeneous structure concept mentioned in the introduction [3]. According to this model, the melt keeps, in a certain temperature region above the melting point, a microheterogeneous state which is inherited from the heterogeneous initial ingot. The dispersed regions or clusters are thus in a metastable equilibrium with the surrounding liquid matrix. The reason is the existence of excess free energy at the border of the clusters; with the decrease of the

cluster radius, this energy grows faster than that of the decreasing interfacial phase surface. In particular, it is anticipated that clusters enriched in boron exist in the melt just after melting. These domains, consisting of iron and of iron, cobalt and/or ternary borides, respectively, are inherited from the microheterogeneous crystalline ingot. The existence of such domains has earlier been reported to exist in Fe-B metallic glasses [2]. The size of these clusters has from thermodynamical calculations been estimated to be of the order of 10 nm [8, 9]. Small angle neutron scattering experiments recently carried out on PbSn melts have confirmed this estimation [10]. The anomaly seen in the viscosity at T_d corresponds thus to the breaking up of boride clusters into smaller ones during heating. These smaller clusters start to dissolve but the melt does not reach a true solution state until a much higher temperature, T_b [3, 14]. However, the length scale of the structural transformation of the microheterogeneous system is such that the dissolution of the clusters greatly influences its rheology and therefore the effective viscosity.

These assumptions are in good agreement with the temperature dependence of the inverse magnetic susceptibility. When the melt is in a two-phase state (i.e. at temperatures lower than about 1400°C for $Fe_{64}Co_{21}B_{15}$ and about 1250°C for $Fe_{85}B_{15}$), the susceptibility can be described by the following equation:

$$\chi(T) = \alpha\chi_\alpha(T) + \beta\chi_\beta(T) \qquad (1)$$

where α and $\chi_\alpha(T)$ are related to the dilute solution of boron in the iron-cobalt matrix and β and $\chi_\beta(T)$ to the behavior of the clusters, respectively. It should be recalled that $\alpha + \beta = 1$. The coefficient β depends only on the relative volume of the clusters enriched with boron and not on their size. The domains start to dissolve at about 1400°C for $Fe_{64}Co_{21}B_{15}$ and about 1250°C for $Fe_{85}B_{15}$ ($\alpha = 1$, $\beta = 0$) and the change in the slope of the $\chi(T)$ curve is observed (Cf. Fig. 3).

From the results on molten alloys reported above and elsewhere [3, 4, 13, 14], it is then natural to expect that amorphous ribbons quenched from a melt, which has been heated above the temperature where the clusters decompose, will have different sizes of microheterogeneities [15, 16] and, consequently, different physical properties [17] as compared to the ones quenched from a melt without overheating. The rest of this paper will be devoted to this phenomenon.

3. Experimental investigations of the amorphous state

3.1. Production of metallic glass ribbons

In order to investigate the effect of the structure and the microstructure, of the melt before quench on their physical properties, several amorphous ribbons were prepared by the planar-flow casting technique with different production conditions at the Institute of Physics, Bratislava, as described elsewhere [17]. The master alloy was put into a quartz crucible with a rectangular orifice 10×0.55 mm at its bottom. The alloy was melted by induction heating and after reaching the appropriate temperature the melt was forced by an excess pressure of about 16 kPa out on a fast-rotating Cu-wheel (520 mm diameter, 115 mm width), rotating at a speed of 1000 rev/min. The distance between the surface of the wheel and outlet nozzle was about 0.17 mm. Three series of ribbons were produced for each alloy. The temperature of the melt, the quenching temperature and the thickness are given in Table I for each ribbon. The melt was kept about five minutes at every temperature in order for it to reach an equilibrium state. The differences in thickness originate from the different values of the viscosity but also on several other production parameters as discussed in [17]. This difference in thickness has to be taken into account in the interpretation of the macroscopic properties, especially the mechanical ones, as discussed in [14]. It should be mentioned that a higher overheating temperature was in principle required for the series II and III [14] but could not be realized with the available type of quenching installation because of technical difficulties [17]. The overheating temperature, used in the production of the samples, is indicated by the black arrows in Figs 1 and 2, while the temperatures from which the different samples have been quenched are indicated by arrows with open heads. The same type of arrow lines (full, dotted and dashed) corresponds to the same sample.

3.2. Investigations by Differential Scanning Calorimetry (DSC)

The Differential Scanning Calorimetry (DSC) experiments, the results of which are shown in Fig. 4 were performed on a Perkin-Elmer DSC7 calorimeter with two different heating rates, 5 and 16 K/min.

The DSC curves for all $Fe_{85}B_{15}$ ribbons exhibit the typical two-peak behavior [18] where the first peak

TABLE I Melt and quenching temperatures of the produced amorphous ribbons

	$Fe_{85}B_{15}$			$Fe_{64}Co_{21}B_{15}$		
	Sample I	Sample II	Sample III	Sample I	Sample II	Sample III
Maximum temperature of melt °C	1250	1350	1400	1270	1350	1350
Quenching temperature °C	1250	1310	1250	1250	1350	1250
Thickness of ribbon μm	30–33	27–29	35–39	30–34	32–36	18–20

corresponds to α-Fe crystallization and the second to the crystallization of Fe_3B or Fe_2B (cf. Fig. 4a). The two crystallization peaks were separated by a least square fitting of two Gaussian functions. The DSC curves for all $Fe_{64}Co_{21}B_{15}$ ribbons exhibit also a two-peak behavior (cf. Fig. 4b). The first peak corresponds in this case to α-FeCo crystallization and the second to the formation of borides [19]. The positions of the maxima of the Gaussian functions T_n^i, where $n = 1$ and 2 means the first and second peak, respectively, and i the heating rate, are given in Tables II and III. The behavior of the three series is, with one minor exception, the same and independent of heating rate for both alloys. The following general trends can be observed:

—Samples of series I, which are quenched at a low temperature without overheating, have a late onset of α-Fe crystallization but an early onset of boride crystallization (cf. Fig. 4a and b).
—Samples of series II, which are quenched from the highest temperature, exhibit the earliest onset of crystallization of α-Fe but the last one for the borides (cf. Fig. 4a and b).
—Samples of series III, which are quenched from a low temperature after overheating, exhibit an early onset of crystallization of both α-Fe and borides (cf. Fig. 4a).
—The shape of the crystallization peak of the borides is different for samples of series II: smaller width and larger height.

TABLE II The positions of the peaks in the DSC curves for $Fe_{85}B_{15}$. T_n^i denotes the temperature at which the nth crystallization process starts at a heating rate of i K/min

Sample	T_1^5 °C	T_2^5 °C	T_1^{16} °C	T_2^{16} °C
1	401.0	439.7	423.7	462.1
2	398.8	441.4	421.0	464.2
3	399.2	439.4	422.3	462.1

TABLE III The positions of the peaks in the DSC curves for $Fe_{64}Co_{21}B_{15}$. T_n^i denotes the temperature at which the nth crystallization process starts at a heating rate of i K/min

Sample	T_1^5 °C	T_2^5 °C	T_1^{16} °C	T_2^{16} °C
1	385.0	480.0	406.9	500.4
2	385.4	483.3	406.9	502.9
3	384.6	482.7	405.8	502.5

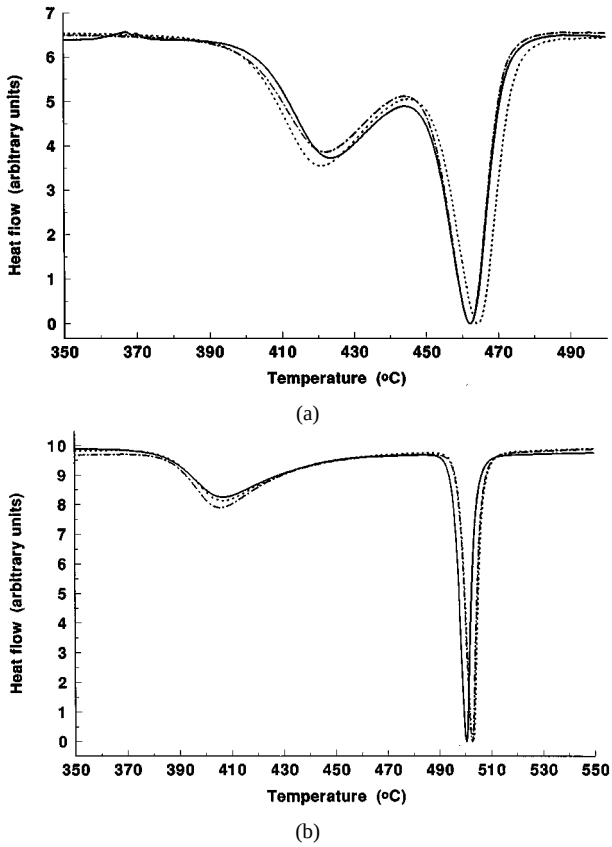

Figure 4 Differential Scanning Calorimetry curves for a) $Fe_{85}B_{15}$ and b) $Fe_{64}Co_{21}B_{15}$ ribbons. Full line—series I; dotted line—series II; dash-dotted line—series III.

3.3. Electrical resistivity

The resistivity ρ was measured by the standard 4-probe method with heating rate of 16 K/min and a linearity of heating better than 0.05%. The results are shown in Fig. 5 where the resistivity is given normalized to the value at 177°C. The accuracy of the measurements was better than 0.01%. The curves, shown in Fig. 6a and b, are the temperature derivatives of the resistivity curves in Fig. 5.

The variation of the measured resistivity for $Fe_{85}B_{15}$, as shown in Fig. 5, is very similar for all ribbons, with a weak temperature dependence and absolute values close to 130 $\mu\Omega$ cm in accordance with earlier measurements [20, 21]. The differences between the alloys are compatible with the estimated error in the determination of ρ. In the amorphous state such a large value of the resistivity and its comparatively weak temperature dependence indicate that the main contribution to the scattering of the conduction electrons is due to atomic short-range order. Two stages of crystallization can also be seen in the resistivity curves, in agreement with Fig. 4a. During the first stage, the resistivity decreases almost with a factor two and in the second about 10% from its initial value. In the crystalline phase, the

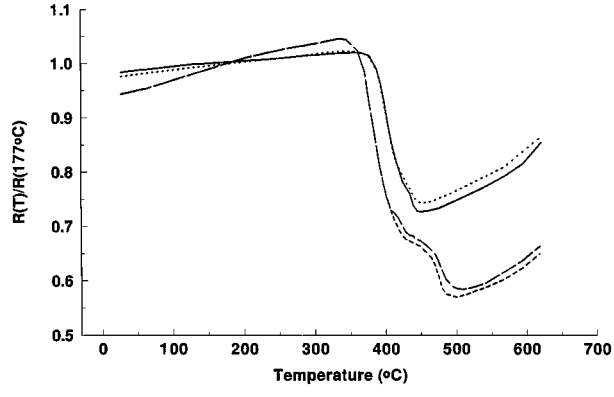

Figure 5 Temperature dependence of the relative electrical resistivity. Full line: $Fe_{85}B_{15}$ series I and III, dotted line: $Fe_{85}B_{15}$ series II. Dashed line: $Fe_{64}Co_{21}B_{15}$ series I and III, long-dashed line: $Fe_{64}Co_{21}B_{15}$ series II.

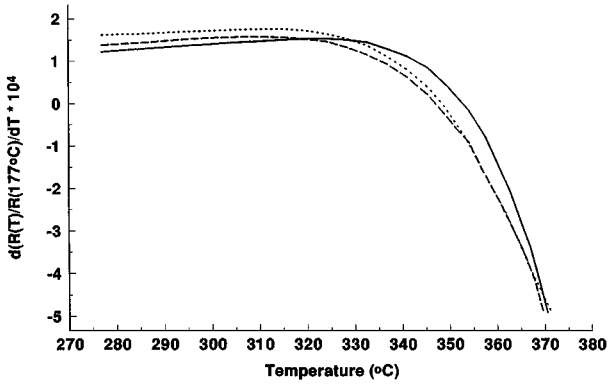

(a)

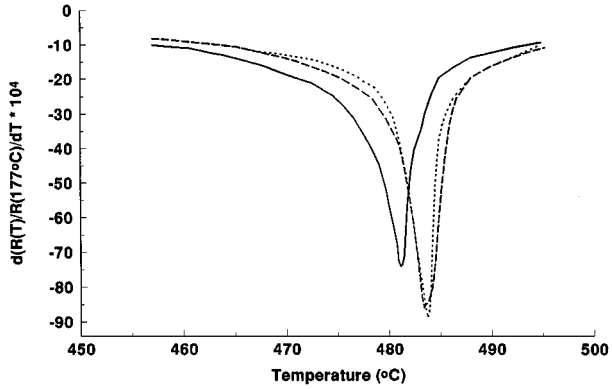

(b)

Figure 6 Temperature dependence of the temperature derivative of the electrical resistivities shown in Fig. 6 for a) $Fe_{85}B_{15}$ and b) $Fe_{64}Co_{21}B_{15}$ ribbons. Full line: series I; dotted line: series II; dashed line: series III.

TABLE IV Saturation induction B_s, remanence B_r and coercivity H_c for $Fe_{85}B_{15}$ ribbons

Property	Sample I	Sample II	Sample III
B_r [Tesla]	1.1	1.36	1.3
B_r [Tesla]	0.3	0.54	0.45
H_c [A/m]	360	260	300

TABLE V Coercivity H_c and remanent magnetization M_r for as-quenched $Fe_{64}Co_{21}B_{15}$ ribbons at different applied fields

	Maximum applied field [A/m]							
	1000		500		150		30	
Sample	H_c	M_r	H_c	M_r	H_c	M_r	H_c	M_r
1	6.8	104	5.8	104	4.3	104	4	103
2	8.5	54	8.5	55	6.7	54	6.1	45
3	5.4	117	5.1	115	4	120	4.1	118

TABLE VI Coercivity H_c and remanent magnetization M_r for $Fe_{64}Co_{21}B_{15}$ ribbons annealed at 280°C for 2 hours in different applied fields

	Maximum applied field [A/m]							
	1000		500		150		30	
Sample	H_c	M_r	H_c	M_r	H_c	M_r	H_c	M_r
1	17.2	62	17.4	62.4	14.9	59.9	12.9	51
2	30.7	31.6	22.4	32.1	16.7	25.5	10.4	9.4
3	9	123	8.9	121.3	6.3	114	6	111.2

temperature dependence of the resistivity is nonlinear, which is typical for ferromagnetic materials. There is also a difference between the different series of alloys, the sample of series II having a lower resistivity. The temperature at which the resistivity is changing drastically is different in the three series of produced ribbons, which indicates that the crystallization process is proceeding according to different routes. Thus, as can be seen in Fig. 6a, the effects of α-Fe crystallization appears several degrees earlier for ribbons from series II and III than for series I which is in agreement with the DSC data presented in Fig. 4a.

In case of $Fe_{64}Co_{21}B_{15}$ two distinct stages of crystallization can also be observed in the $\rho(T)$ curves, also shown Fig. 5. The first one, which corresponds to the formation of α-solid solution of boron in an iron-cobalt-boron matrix begins for all ribbons at the same temperature and it is accompanied by a resistivity decrease of about 30% from the initial value. During the second stage (i.e. boride crystallization) an additional resistivity decrease of about 10% is observed. Fig. 6 presents the temperature derivatives of the part of Fig. 5 corresponding to the second step crystallization (borides). The same trends as seen in the DSC measurements can be observed: The samples of series I exhibit the earliest stage of boride crystallization.

3.4. Measurements of magnetic properties

The saturation induction B_s, the remanence B_r and the coercivity H_c as well as their variation with annealing time were measured for all alloys. The results for the as-quenched $Fe_{85}B_{15}$ samples are given in Table IV. For all quantities sample II have the most favorable values: largest induction and lowest coercivity. For some quantities the difference between series II and III are rather small. During exposition the decay of the magnetic remanence is highest for sample I and much weaker for samples II and III.

The effect of annealing on the coercivity and the remanent magnetization for the $Fe_{64}Co_{21}B_{15}$ alloys are given in Tables V and VI. Measured values for the as-quenched samples are given in Table V while the ones measured after 2 hours annealing at 280°C are shown in Table VI. Sample III has in this case the largest value of the remanence and the smallest value of the coercivity both in the as-quenched and the annealed states. The effect of annealing is also much smaller for sample III. The corresponding hysteresis loops are shown in Fig. 7.

4. Discussion

The comparative analysis of the data presented above allows to conclude that the various heat treatments of the melt influence the properties of rapidly quenched amorphous ribbons significantly. Besides, it also gives some opportunity to interpret the mechanisms responsible for the transformations taking place in $Fe_{85}B_{15}$ and $Fe_{64}Co_{21}B_{15}$ melts around T_d.

In the binary system $Fe_{85}B_{15}$ the anomalous changes in the viscosity and surface tension in the melt at

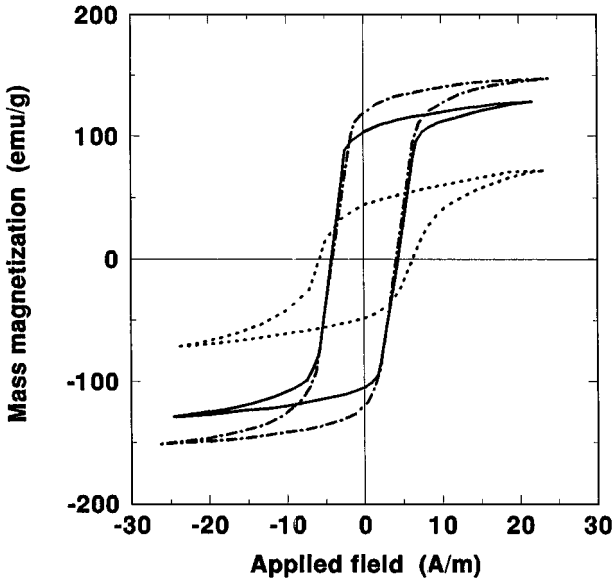

Figure 7 Measured hysteresis loops for $Fe_{64}Co_{21}B_{15}$ ribbons. Full line—series I; dotted line—series II; dash-dotted line—series III.

$T_d = 1300°C$ do not correlate with the smooth temperature dependence of the magnetic susceptibility. Taking into account that the last property is determined mainly by short range ordering in the liquid alloy it can be concluded that the short-range order does not change at T_d. This is confirmed by the fact that the electrical resistivity measured for these ribbons is very similar. On the contrary, the properties of the ribbons sensitive to their meso-scale microheterogeneity (crystallization temperatures and activation energies, rate of crystallization process, magnetic properties) change significantly. Therefore, it is obvious that some kind of meso-scale transformation takes place at the temperature T_d. The temperature, T_b, characteristic of the transformation process of the melt from a metastable microheterogeneous state to a true solution is found around 1600°C in the Fe-B system [11]. One can thus conclude that when heated above 1400°C, the liquid $Fe_{85}B_{15}$ alloy transforms from an initial microheterogeneous state to another one with the same or similar short-range order but not to the state of true solution. What is happening during a subsequent cooling is not yet fully understood. It can be supposed that heating to a temperature above T_b induces an irreversible transformation to the state of true solution. A subsequent cooling will thus conserve this state. It can be conjectured that this has not occurred in any of the studied ribbons because of technical problems during the production (no overheating above T_b was carried out). This conjecture has recently been discussed in terms of TTT diagrams in [17]. From all results both structural, microstructural and macroscopic, reported in this work and elsewhere on different kinds of ribbons [15, 17], a subsequent cooling after a heat treatment of the melt at a temperature between T_d and T_b can thus be interpreted by two possible mechanisms:

—The dissolution process taking place above T_d is irreversible: The melt will thus during a subsequent cooling preserve the state of dissolution of the microheterogeneities it has reached in the heating process. The increase of the viscosity with decreasing temperature is then governed by an activation energy, similar in magnitude to the one governing the viscosity increase shown in Fig. 1. Accordingly the viscosity values are then following curves nearly parallel to, but above, the cooling curves in Fig. 1.

—The dissolution process taking place above T_d is reversible: The viscosity during a subsequent cooling would then follow the heating curves in Fig. 1.

Although the first interpretation seems to be most plausible, it is not possible to reach a clear and unambiguous conclusion as it was not possible to reach high enough temperatures in the available melt spinning installation [17]. However, it has been observed that when reheated, after a heat treatment at a temperature below T_b but above T_d and a following solidification, the size and the amount of microheterogeneities in a PbSn melt of eutectic composition were decreased [10].

In the ternary system $Fe_{64}Co_{21}B_{15}$ the anomalous changes of the viscosity and the surface tension occurs also at $T_d = 1300°C$ and a similar discussion as for $Fe_{85}B_{15}$ above can be performed. However, in this case the inverse magnetic susceptibility, contrary to what was the case for $Fe_{85}B_{15}$, exhibits an anomalous temperature variation but at a lower temperature than T_d, at about 1180°C. It can thus be concluded that in this case some changes of the short range order of the melt precedes the transformation of the initial meso-scale microheterogeneity. The most probable mechanism of such transformation can be a rearrangement of atoms in the clusters. At T_d a dissolution of disperse particles inherited from the inclusions of the ternary compound into particles of binary compounds of stochiometric compositions starts. This hypothesis is confirmed by the absence of any sign of a ternary compound crystallization in the DSC curves from the samples heated up to 1350°C. When cooling the melt after its heating above this temperature the particles of the ternary compound are not reappearing which is in favor of the irreversible interpretation, mentioned above for $Fe_{85}B_{15}$ alloys.

As outlined above, all the effects discussed earlier would have been much more accentuated for both alloys if the melts could have been overheated above T_b before the quench [17]. Unfortunately such overheating was not possible. An estimation of the production conditions has been made in terms of Time-Temperature-Transformation (TTT) curves for the Fe-Co-B alloys, stressing the strong influence of a non-complete control of the production conditions, especially the overheating temperature and the cooling rate, on the quality of the produced ribbons [17]. The TTT curves have been derived from the knowledge of some production parameters and from detailed investigations of the structure and the microstructure of the three series of samples by neutron diffraction and neutron small angle scattering [15]. The conclusions reported in [15] concerning the influence of the state of the melt before quench on the nature, size and amount of clusters and particles in the produced ribbons are in complete agreement with the interpretation of the measurements in the liquid state presented above. Another study devoted to

the Ni-P system has also been carried out and similar conclusions have been arrived at [15–17].

5. Conclusions

From the results presented above, it can be concluded that there exists in some eutectic and near-eutectic melts a temperature domain, defined by the two temperatures, T_d and T_b. At temperatures below T_d the melt contains microheterogeneities inherited from the initial ingot. At T_d these inhomogeneities start to dissolve. Whether this dissolution process is reversible or irreversible is still not fully clear. The dissolution proceeds until a temperature T_b where the melt reaches the state of true solution. All the obtained results confirm the theoretical developments presented in [4]. The metallic glass ribbons obtained by rapid quench from different states of the melt have substantially different structure, crystallization behavior, magnetic and other macroscopic properties.

Acknowledgement

The authors are thankful to the Swedish Institute for the financial support which made part of this work possible. Thanks are also due to D. Janičkovič for his help in the production of the amorphous ribbons and the resistivity measurements during the visit of VES in Bratislava.

References

1. V. P. MANOV, S. I. POPEL and P. I. BULER, *Rasplavy (Melts)* **1** (1989) 23 (in Russian).
2. V. P. MANOV, S. I. POPEL, P. I. BULER, A. B. MANUKHIN and D. G. KOMLEV, *Mat. Sci. Eng.* **A133** (1991) 535.
3. P. S. POPEL, O. A. CHIKOVA and V. M. MATVEEV, *High Temp. Mat. Proc.* **14** (1995) 219.
4. P. S. POPEL and V. E. SIDOROV, *Mat. Sci. Eng.* **A226-228** (1997) 237.
5. A. C. MITUS and A. Z. PATASHINSKI, *Physica* **A150** (1988) 383.
6. J. A. KNAPP and D. M. FOLLSTAEDT, *Phys. Rev. Lett.* **58** (1987) 2454.
7. R. GOSWANI and K. CHATTOPADHYAY, *Mat. Sci. Eng.* **A179/A180** (1994) 163.
8. V. M. BARBOI, Y. M. GLASMAN and G. I. FUKS, *Coloidnyo Zhurnal USSR* **32** (1970) 233.
9. P. S. POPEL and B. BAUM, *Metally* **5** (1986) 47 (in Russian).
10. P. S. POPEL, V. E. SIDOROV, M. CALVO-DAHLBORG, U. DAHLBORG, V. P. MANOV, E. BROOK-LEVINSON and V. MOLOKANOV, submitted.
11. P. S. POPEL, E. L. ARKHANGELSKY and V. V. MAKEJEV, *Vysokotemperaturnye Rasplavy (High Temperature Melts)* **1** (1995) 85 (in Russian).
12. V. V. MAKEJEV and P. S. POPEL, *Zh. Phys. Chim. (USSR)* **64** (1990) 568.
13. V. E. SIDOROV, P. S. POPEL, L. SON and L. MALYSHEV, *Mat. Sci. Eng.* **A226–228** (1997) 317.
14. M. CALVO-DAHLBORG, *ibid.* **226–228** (1997) 833.
15. U. DAHLBORG and M. CALVO-DAHLBORG, in Proc. Int. Workshop on Mechanical Properties of Metallic Glasses, 22–24 Sept. 1998, Kosice, Slovakia, p. 17.
16. U. DAHLBORG, M. CALVO-DAHLBORG, R. K. HEENAN, J. M. RUPPERT, P. S. POPEL and V. E. SIDOROV, submitted.
17. M. CALVO-DAHLBORG and J. M. RUPPERT, in Proc. Int. Workshop on Mechanical Properties of Metallic Glasses, 22–24 Sept. 1998, Kosice, Slovakia, p. 9.
18. U. KÖSTER, in "Phase Transformations in Crystalline and Amorphous Alloys," edited by B. L. Mordike (DGM, 1982) p. 113.
19. W. HOFSTETTER, H. SASSIK, R. GRÖSSINGER, R. TRAUSMUTH, G. VERTESY and L. F. KISS, *Mat. Sci. Eng.* **A226–228** (1997) 213.
20. K. DEHGHAN, J. M. DUBOIS, G. LECAËR and C. TÊTE, *J. Non-Cryst. Solids* **65** (1984) 87.
21. M. ARSHED, M. SIDDIQUE, M. ANWAR-UL-ISLAM and N. M. BUTT, *Solid State Comm.* **89** (1994) 101.

Received 20 January
and accepted 5 October 1999